ACS APPLIED MATERIALS & INTERFACES

Research Article

www.acsami.org

Nanoporous PtCo Surface Alloy Architecture with Enhanced Properties for Methanol Electrooxidation

Huajun Qiu*[,†,‡] and Feixue Zou[†]

[†]School of Chemistry and Chemical Engineering, Shandong University, Jinan 250100, China

[‡]School of Chemical and Biomedical Engineering, Nanyang Technological University, 70 Nanyang Drive, Singapore 637457, Singapore

Supporting Information

ABSTRACT: By selectively dealloying a PtCoAl ternary alloy, a novel nanoporous PtCo (np-PtCo) alloy with a three-dimensional bicontinuous pore-ligament structure is successfully fabricated. X-ray diffraction and electron microscopic characterizations demonstrate the single-crystal nature of the alloy ligament with a ligament size down to ~3 nm. After a mild electrochemical dealloying process, a nanoporous near-surface alloy structure with a Pt-rich surface and a PtCo alloy core is obtained. Electrochemical measurements show that the np-PtCo surface alloy has greatly enhanced catalytic activity and durability toward methanol electrooxidation compared with a state-of-the-art Pt/C catalyst. The peak current density of methanol electrooxidation on a np-PtCo surface alloy is more than 5 times of that on Pt/C. More importantly, continuous potential cycling from 0.6 to 0.9 V (vs RHE) in a 0.5 M H_2SO_4 aqueous solution demonstrates that a np-PtCo surface alloy has excellent structure stability, with more than 90% of the initial electrochemical active surface area (EASA) retained after 5000 potential cycles. Under the same conditions, the EASA of Pt/C drops to ~70%. With evident advantages of facile preparation as well as enhanced electrocatalytic activity and durability, a np-PtCo surface alloy nanomaterial holds great potential as an anode catalyst in direct methanol fuel cells.

KEYWORDS: *dealloying, structure stability, bimetallic catalysts, fuel cell*

INTRODUCTION

Electrochemical oxidation of methanol has attracted much attention because of the great potential of direct methanol fuel cells. Platinum-based nanomaterials are currently the most investigated catalysts for methanol electrooxidation because of their high electrocatalytic activities.[1−9] Currently, the state-of-the-art commercial catalyst for methanol oxidation reaction (MOR) is Pt/C [platinum nanoparticles (Pt-NPs) with a size of ~3 nm dispersed on a carbon support].[3] However, the mass activity of the Pt/C catalyst is still not that satisfactory, and an even more serious problem for Pt/C catalysts is their lack of long-term stability resulting from corrosion of the carbon support and the weak interaction between Pt-NPs and the support. It has been reported that, under long-term fuel-cell operation conditions, Pt-NPs on the carbon support would undergo aggregation, Oswald ripening, and poisoning, which could cause a significant loss of the electrochemical active surface area (EASA) and catalytic activity.[10]

While most researches have focused on enhancing the performance of Pt/C-like carbon-supported catalysts,[7,11−13] more recently supportless Pt catalysts (especially one-dimensional Pt nanostructures) are found to exhibit intriguing properties with evidently alleviated loss in the EASA.[14−16] For example, Pt and PtPd nanotubes,[14] a multiarmed Pt nanowire,[15] and a Pt nanowire membrane[16] have been reported to have improved activity and durability for oxygen reduction reaction (ORR) compared with commercial Pt/C. However, because of their relatively large feature dimension (usually above 5 nm), most of these catalysts only show mild mass-specific-activity enhancement compared with a commercial Pt/C catalyst.[17] To further improve the mass specific activity, Wong and co-workers prepared ultrathin Pt nanowires with a diameter of ~1.3 nm by chemically reducing $PtCl_6^{2-}$ in organic solutions.[18] Sun and co-workers synthesized thin FePtPd alloy nanowires with a diameter of 2.5 nm by thermal decomposition of $Fe(CO)_5$ and sequential reduction of $Pt(acetylacetonate)_2$ and $Pd(acetylacetonate)_2$ at high temperature (160−240 °C) in organic media.[19] Shui and co-workers prepared nanoporous PtFe nanowires with ligament sizes of 2−3 nm by the combination of electrospinning and chemical dealloying.[20] Another strategy to improve the Pt mass activity is the fabrication of a core−shell nanostructure with a thin Pt shell. For example, by Cu underpotential deposition followed by Pt replacement, Pt-monolayer-coated ultrathin Pd nanowire core−shell structures showed significantly enhanced mass specific activity and durability compared with a commercial Pt/C catalyst.[21,22] Although these results are very promising, as far as we know, the facile and large-scale preparation of new free-standing catalysts of practical value with high mass specific activity and durability is still challenging.

It is known that alloying Pt with transition metals can improve its catalytic activity and CO tolerance because of modification of the Pt electronic structure as well as correlation of the ligand and strain effects.[23−26] For instance, alloying Pt with Co can generate promising cathode electrocatalysts for ORR with reduced catalyst cost and high OH resist-

Received: November 26, 2011
Accepted: February 14, 2012
Published: February 24, 2012

ance.[3,5,17,27,28] Meanwhile, a PtCo alloy also shows some exceptional properties toward other catalytic reactions such as CO oxidation.[29] However, there is still some controversy about the performance of the PtCo catalyst in MOR. Some authors report that MOR on Pt is favored by the presence of Co; however, others have the opposite conclusion. By studying the catalytic activities of PtCo/C and PtCoW/C toward MOR in an acidic environment, Zeng and Lee[30] found that the addition of Co promoted methanol dehydrogenation, resulting in better catalysts for MOR compared to Pt/C. While Gojkovic[31] reported that the rate of MOR on Pt_3Co/C was not superior to that on Pt/C in acidic solutions. Salgado and co-workers[32] also found that the onset potential for MOR on PtCo/C shifted toward more positive potentials compared with that on Pt/C; i.e., the presence of Co was detrimental for MOR. Rojas et al.[6] reported that although the addition of Co improved the CO_2 efficiency, the current density of methanol oxidation on the bimetallic catalysts was lower than that recorded on the monometallic samples. It is believed that the different preparation strategies with different additives will result in catalysts with different surface states, which should be responsible for their different catalytic activities toward MOR. In addition, the different supports for the catalysts and their interaction may also contribute to their different performances. Therefore, the preparation of a free-standing PtCo alloy catalyst with a uniform structure and clean surface is also very important for the study of the effect of Co on the catalytic activity of Pt for MOR.

Dealloying (i.e., selectively removing one or more active metals from alloys) has been proven to be very effective in producing free-standing three-dimensional (3D) nanoporous metal catalysts in large amountd.[33−43] A series of nanoporous metals (Pt, Pd, Au, Ag, Cu, etc.) have been successfully fabricated by dealloying these metal-based binary alloys.[41] One of the most famous exampled is nanoporous gold obtained by dealloying a AuAg alloy, which possesses extraordinary physicochemical properties.[33,34,37] However, it is noticed that the fabrication of advanced nanoporous alloy materials (especially noble and non-noble metal alloys) by this simple dealloying strategy is still challenging,[2,44,45] although nanoporous alloys can be prepared by dealloying binary precursor alloys.[2,46,47] The bimetallic ratio of the resulting nanoporous alloy is hard to control. A wise choice is to design a ternary precursor alloy. Upon dealloying the ternary alloy, only one component can be selectively removed while the other two are well-preserved. In this way, the bimetallic ratio of the resulting nanoporous alloy can be well-controlled by the feed ratio of the precursor alloy.

In the current work, we report the design of a PtCoAl ternary precursor alloy with a predetermined alloy composition and the fabrication of a nanoporous PtCo (np-PtCo) alloy with a uniform alloy ligament (~3 nm) and a bimetallic ratio by selectively dealloying the precursor alloy. Considering recent studies that demonstrate that the catalytic activity can be further improved on a fine-tuned Pt near-surface structure with a nearly pure Pt surface and alloy subsurface configuration (also called a surface alloy),[5,23,48,49] the as-prepared np-PtCo is further dealloyed by a mild electrochemical treatment to fabricate a np-PtCo surface alloy. Electrochemical measurements show that the novel nanoporous surface alloy nanocatalyst exhibits remarkably improved catalytic activity and durability toward MOR compared with a commercial Pt/C catalyst.

EXPERIMENTAL SECTION

Ternary PtCoAl alloy foils with a thickness of ~50 μm were prepared by refining pure (>99.9%) Pt, Co, and Al in an arc furnace, followed by melt spinning under an argon-protected atmosphere. A np-PtCo alloy was prepared by selectively dealloying the ternary alloy in a 1.0 M NaOH solution at room temperature for 24 h. The np-PtCo surface alloy structure was prepared by electrochemically dealloying the as-prepared np-PtCo in 0.5 M H_2SO_4 by cyclic voltammetry (CV) cycling from 0 to 1.3 V for 20 cycles. The E-TEK Pt/C catalyst was purchased from Aldrich with metal loading of 20 wt % on carbon powder.

X-ray diffraction (XRD) data were collected on a Bruker D8 Advanced X-ray diffractometer using Cu Kα radiation (λ = 1.5418 Å) at a scan rate of 0.04° s^{-1}. The microstructures were characterized on a JEM-2100 high-resolution transmission electron microscope and a JSM-6700 field-emission scanning electron microscope equipped with an Oxford INCA x-sight energy-dispersive X-ray spectrometer.

All electrochemical experiments were performed on a CHI 760C workstation in a three-electrode cell with a modified electrode as the working electrode, Pt foil as the counter electrode, and mercury sulfate as the reference electrode. All potentials were referred to RHE. The catalyst suspensions were made by mechanically mixing 2.0 mg of catalyst, 2.0 mg of carbon powder, 300 μL of isopropyl alcohol, and 100 μL of a Nafion solution (5 wt %). The catalyst loadings on a polished 4-mm-diameter glassy carbon electrode were 20 μg for np-PtCo and 8 μg for Pt/C. Electrolyte solutions were deoxygenated by bubbling with high-purity N_2 for at least 30 min prior to measurements. CO-stripping experiments were carried out by first holding the thus-made electrodes at 0.15 V (vs RHE) in a 0.5 M H_2SO_4 solution with continuous CO bubbling for 20 min. The electrode was then transferred into a 0.5 M N_2-purged H_2SO_4 solution to record the CO-stripping profiles. The EASA of Pt was calculated by integrating the charge associated with hydrogen adsorption.[2]

RESULTS AND DISCUSSION

Preparation and Characterization of np-PtCo. We choose an Al-based ternary alloy as the precursor alloy because of its active properties and rich supply of Al. The atomic percentage (atom %) of Al is set at 80% to facilitate chemical dealloying. On the basis of previous reports that for PtCo alloy electrocatalyst the optimal atomic percentage of Co is usually in the range from 30 to 40 atom %,[17] in this work the atom percentage of Pt and Co in the ternary alloy are controlled at 13% and 7%, respectively. Thus, the content of Co in the resulting sample should be 35 atom % after the removal of Al from the $Pt_{13}Co_7Al_{80}$ alloy in a 1.0 M NaOH aqueous solution (a detailed study on the effect of the Co content is not included in this work). Energy-dispersive X-ray spectrometry (EDS) characterization (Figure S-1a in the Supporting Information, SI) of the ternary precursor alloy demonstrates that the ratio of the three components is almost the same as the initial feed ratio. After 24 h of dealloying, the EDS result shows that Al is etched to an undetectable level while the contents of Pt and Co are unchanged (Figure S-1b in the SI), indicating excellent control of the composition of the resulting sample by this method. Because the formation of the PtCo catalyst is not based on chemical coreduction of the respective source metal ions, this process can achieve a nearly 100% yield with essentially no precious metal loss. More importantly, this process can predecide the chemical composition of the resulting alloy. This is also in sharp contrast to the traditional approach of chemical reduction, where the feed ratio of metal salts does not guarantee the same nominal composition in the final alloy sample, mainly because of the different reducing capacities of individual elements.

XRD is used to examine the phase structures of the PtCoAl ternary alloy and the dealloyed sample (Figure 1). For the

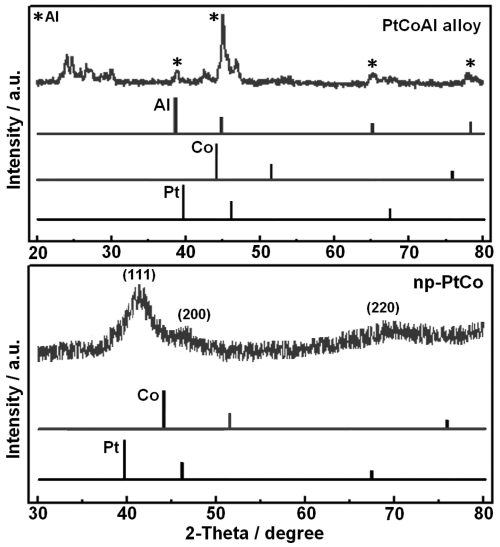

Figure 1. XRD patterns of the PtCoAl ternary alloys before and after dealloying.

ternary alloy, because of the large content of Al, a pure Al phase exists (marked with an asterisk). The other diffraction peaks are complex and can be ascribed to different Al-based alloy phases such as Al21Pt6, Al6Pt, Al13Co4, Al5Co2, etc., indicating the preferential formation of Al-rich alloy phases (probably because of the large content of Al) and the coexistence of multiple alloy phases in the precursor alloy. However, it is interesting to find that, after 24 h of dealloying, accompanied by the complete removal of Al, a uniform PtCo alloy structure is obtained. One can see from Figure 1 that the dealloyed sample shows a set of three diffraction peaks that are assigned to the (111), (200), and (220) reflections of a face-centered-cubic structure. The broad diffraction feature is mainly due to the large surface stress developed during dealloying.[50] No diffraction peaks from pure Co (or its oxides) as well as ordered PtCo alloy phases are observed, which suggests the formation of a disordered single-phase PtCo alloy. Compared with the standard diffraction pattern of Pt, all diffraction peaks from the dealloyed sample shift to higher angles because of the substitution of smaller Co atoms in the Pt crystal lattice. Notably, the diffraction peak from the (111) diffraction is more pronounced, while those from the (200) and (220) diffractions are very weak. This indicates that the PtCo alloy is primarily dominated by (111) facets.

Figure 2a shows the scanning electron microscopy (SEM) image of the dealloyed sample that is composed of hundreds of PtCo nanorods. The PtCo nanorods are several micrometers in length and hundreds of nanometers in diameter. Furthermore, these rods are surprisingly parallel with each other in a certain range, forming clusters. For clarity, two parallel clusters are highlighted by the dot-dashed lines. The SEM image with a higher magnification (Figure 2b) shows that the nanoporous structure can be clearly observed on the surface of the PtCo nanorods. The clear contrast between the dark skeletons and bright pores in the transmission electron microscopy (TEM) image of the nanorod (Figure 2c) further reveals the bicontinuous ligament/pore structure in the interior of the PtCo nanorods, and the length scale of the ligaments/pore is

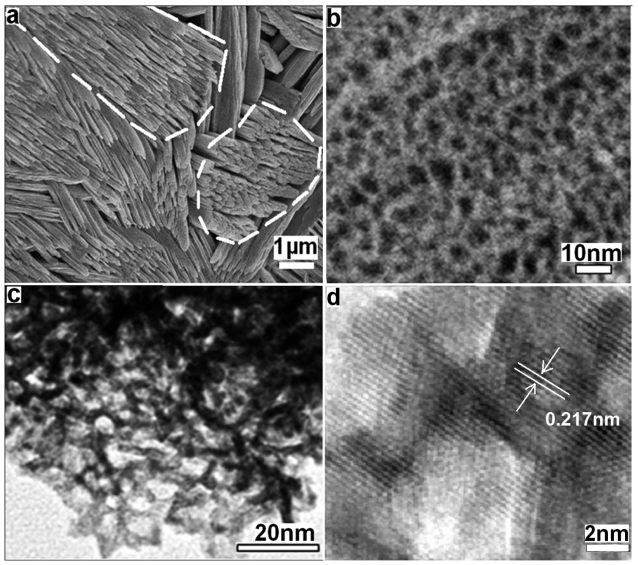

Figure 2. SEM (a and b), TEM (c), and HRTEM (d) images of np-PtCo.

~3 nm. The high-resolution TEM (HRTEM) image (Figure 2d) provides more detail for the alloy ligament, in which the continuous lattice fringes are well-resolved around the whole pore, indicating the formation of single-crystalline interconnected ligaments. It is noted that the exposed facets are along the (111) planes with the lattice spacing measured to be 2.17 Å, which is in accordance with the value calculated by Vegard's law. The result that most exposed facets are along the (111) planes is also in excellent agreement with that obtained from the XRD study.

It is very interesting to find that, by simple dealloying of the PtCoAl ternary alloy, an aligned nanoporous nanorodlike structure with a uniform PtCo alloy ligament can be successfully fabricated. The dealloying process has been widely studied in previous work. Most of these studies are focused on the dealloying of the binary alloy with a single-phase solid solubility across all compositions such as the AgAu alloy.[33] The formation mechanism has been discussed according to a corrosion disordering/diffusion reordering model, a dynamic roughening transition model, and a kinetic Monte Carlo model.[51,52] However, in the present case, for the PtCoAl ternary alloy with multiple alloy phases, the dealloying process and formation mechanism of the aligned nanoporous nanorodlike structure are obviously more complicated. We assume that the dealloying of the ternary alloy started first with the pure Al phase (the most active phase). The removal of the pure Al phase would result in the formation of the large channels between nanorods. The formed large channels can facilitate diffusion of the dealloying solution and the further dealloying of different Al-based alloy phases. Accompanied by the removal of Al from these Al-based alloy phases, the left Co and Pt adatoms on the alloy/solution interface will interdiffused to form PtCo alloy ligaments and nanopores. It is reasonable to believe that these different Al-based alloy phases should be very close to each other. Thus, the lattice vacancy formed by the removal of Al from PtAl (CoAl) phases will be quickly filled by the nearby Co (Pt) adatoms, which results in the formation of a uniform np-PtCo alloy instead of a hybrid of nanoporous Pt and nanoporous Co. To explain the formation of the nanorodlike structure, it is quite possible that, in the precursor PtCoAl alloy,

these Al-based alloy phases exist in the form of nanorods, and after dealloying, the nanorodlike structure is maintained.

Electrocatalytic Performance of np-PtCo toward MOR. To prepare a np-PtCo near-surface alloy structure, the as-prepared np-PtCo is further electrochemically dealloyed in 0.5 M H_2SO_4 by CV cycling from 0 to 1.3 V for ~20 cycles. Figure S-2a in the SI shows the CV curves of the electrochemically dealloyed np-PtCo and commercial Pt/C in a 0.5 M H_2SO_4 solution. The CV curve of np-PtCo (untreated) is shown in Figure S-2b in the SI. Compared with np-PtCo (untreated), the electrochemically dealloyed np-PtCo sample (i.e., a np-PtCo surface alloy) shows more characteristic hydrogen underpotential adsorption/desorption (0−0.4 V) and Pt oxidation (above 0.8 V) curves, which indicates that the np-PtCo surface alloy has a surface state close to pure Pt. Notably, compared with that of Pt/C, the redox waves of the np-PtCo surface alloy are shifted to more positive potentials, suggesting the delayed formation and weakening of Pt-oxygenated species on the np-PtCo surface alloy. It should be mentioned that, after electrochemical dealloying, EDS analysis shows that the content of Co only slightly decreased (~5 atom % decrease), indicating that dealloying only occurs on the outer surface of the alloy ligament. SEM characterization shows that the no obvious changes are observed after mild electrochemical dealloying. The reason for the electrochemical dealloying only occurring on the outer surface of the alloy ligament should be due to the large content of noble metal Pt (~65 atom %), which is over the threshold for complete dealloying of Co.[53]

Figure 3a presents the CV curves of the np-PtCo surface alloy, np-PtCo (untreated), and commercial Pt/C catalyst in a 0.5 M H_2SO_4 + 1.0 M CH_3OH solution. For all three samples, the peak at about 0.90 V in the positive-going scan is attributed to the electrooxidation of methanol. The anodic peak at about 0.75 V in the reverse scan can be associated with the reactivation of oxidized Pt.[12] It is noticed that the peak potentials in the positive-going scan on the two np-PtCo samples locate at 0.90 V, which is evidently lower than that on Pt/C (0.92 V), indicating the facilitated reaction kinetics for methanol dehydrogenation on the nanoporous samples. The enlarged positive scan curve from 0.4 to 0.6 V (inset of Figure 3a) also shows that the methanol oxidation on the two np-PtCo samples starts quickly when the potential is above 0.4 V, while on Pt/C, the current from methanol oxidation has a relatively quick increase until the potential is over 0.5 V. More importantly, the surface specific current density for MOR on the np-PtCo surface alloy is much higher than that on the Pt/C catalyst (more than 5 times). The np-PtCo surface alloy also shows higher activity for MOR compared with np-PtCo (untreated), indicating that the formation of a Pt-rich surface and PtCo alloy core structure is beneficial for further activity enhancement. Figure 3b shows the mass specific activities of the three samples, and the np-PtCo surface alloy still exhibits the highest activity, which suggests that the Pt loading can be markedly reduced if the np-PtCo surface alloy replaces the currently widely used Pt/C as the anode catalyst.

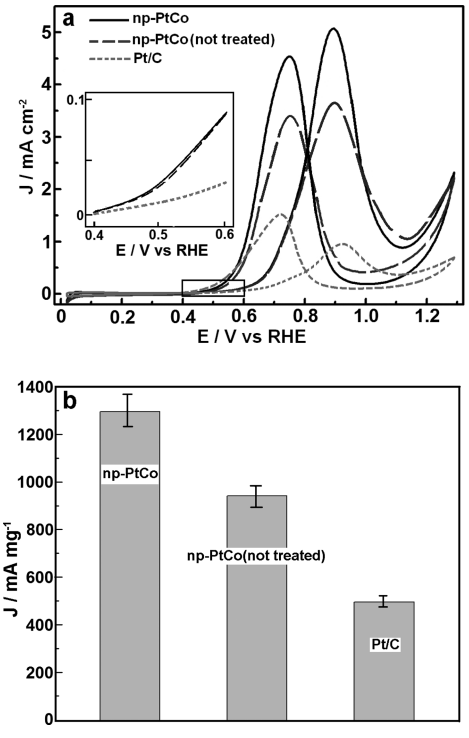

Figure 3. CV curves of the np-PtCo surface alloy, np-PtCo (untreated), and Pt/C catalysts in a 0.5 M H_2SO_4 + 1.0 M CH_3OH solution (a). Inset in a: enlarged image (0.4−0.6 V) during the positive scan; Pt mass specific current densities of the three samples at 0.9 V (b). Scan rate: 50 mV s^{-1}.

To explain the enhanced electrocatalytic activities of PtCo alloys for MOR, two possible mechanisms have been proposed. One is the bifunctional mechanism where Co surface sites allow the formation of oxygenated species to oxidize the dissociative intermediates produced on nearby Pt sites.[4] The other is based on electronic and strain effects through alloying with Co.[24] In this work, because the Pt-rich near-surface alloy structure has a much higher catalytic activity compared with untreated np-PtCo, we assume that the activity enhancement in this work can be better explained by the latter one. Recently, on the basis of both experimental studies and theoretical calculations, Mavrikakis et al.[54] proved that a PtCu near-surface alloy is a promising catalyst for low-temperature water−gas-shift reaction. Strasser et al.[23,55,56] reported that dealloyed PtCu alloy nanoparticles are excellent electrocatalysts for oxygen reduction. The excellent catalytic activity was suggested to be related to a compressively strained Pt-rich shell. By establishing the activity−strain relationship,[23] they demonstrated experimentally that deviation of the Pt-shell lattice parameter from that of bulk Pt (i.e., lattice strain in the shell) is the controlling factor in the activity enhancement of the surface alloy structure. On the basis of these arguments, it is not surprising that the present nanoporous surface alloy structure exhibits enhanced catalytic activity toward MOR. On the other hand, the unique bimodal porous structure with big channels and nanopores is suggested to play a vital role in terms of the easy transport of electrons and medium molecules in all three dimensions.

To gain more insight into the enhanced activity of the np-PtCo surface alloy, a CO-electrostripping experiment was carried out. As shown in Figure S-3 in the SI, CO stripping on the np-PtCo surface alloy displays a markedly negative-potential shift compared with that on Pt/C. The corresponding main peak potentials locate at 0.69 V for the np-PtCo surface alloy and 0.83 V for Pt/C. The peak current density for CO electrooxidation on the np-PtCo surface alloy is smaller than that on Pt/C. These results indicate that CO adsorption is much weaker on the np-PtCo surface alloy than on Pt/C. In other words, the np-PtCo surface alloy is more tolerant to CO

poisoning. Weak CO adsorption should be due to the electronic effect between Pt and Co and the strained Pt surface. These effects may cause a decay of the Pt−CO binding energy and enhance the removal of intermediates from methanol electrooxidation.[6] In addition, a small but clearly discernible CO oxidation feature in the so-called preignition potential region (indicated by an arrow in Figure S-3 in the SI) is observed on the np-PtCo surface alloy but is absent on Pt/C. CO oxidation in the preignition potential region has also been observed on ultrathin Pt nanowires[57] and a well-ordered Pt surface with defect sites[58] and has been attributed to the presence of certain surface sites that are active for CO oxidation. CO oxidation at this low potential region will free more surface sites for methanol adsorption and oxidation, resulting in an enhanced MOR activity. This low-potential CO oxidation also explains why the main CO-oxidation peak on the np-PtCo surface alloy is smaller than that on Pt/C.

The long-term catalytic activity of the np-PtCo surface alloy is also evaluated by studying their steady-state current response with time. Figure 4 presents the chronoamperometry data

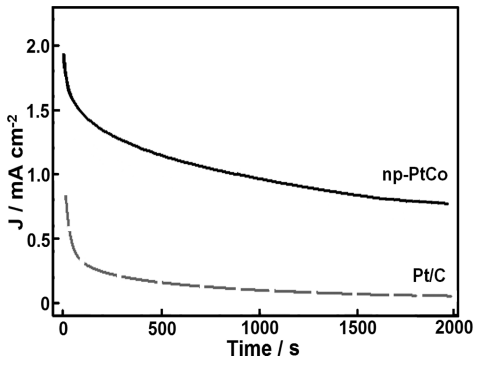

Figure 4. Chronoamperograms for the np-PtCo surface alloy and Pt/C catalysts in a 0.5 M H_2SO_4 + 1.0 M CH_3OH solution at 0.8 V at room temperature.

under 0.8 V in a solution of 0.5 M H_2SO_4 + 1.0 M CH_3OH for 2000 s. At the beginning, the rapid current decay for the two catalysts is caused by the formation of double-layer capacitance. Then the decrease in the current should be due to a small amount of CO_{ads} species accumulation on catalyst surfaces during methanol oxidation.[59,60] In addition, SO_4^{2-} adsorption on the catalyst surface also leads to the current decay by inhibiting the reaction active sites.[61] Upon long-time operation, the current gradually reached a quasi-equilibrium steady state. In comparison, the steady-state current on the np-PtCo surface alloy is much higher than that on a Pt/C catalyst, which is in good agreement with the results from the CV study and indicates that the nanoporous surface alloy has dramatically enhanced catalytic durability.

For practical applications, the structure stability of electrocatalysts during long-term operation is also very important. Therefore, we evaluated the structure stability of the np-PtCo surface alloy by continuous CV cycling from 0.6 to 0.9 V in a 0.5 M H_2SO_4 solution at room temperature. As shown in Figure 5, the EASA of the np-PtCo surface alloy decreases slowly with increasing scan cycles and remains more than 90% of the initial value after 5000 CV cycles, whereas after the same treatment, the EASA of Pt/C drops to ~74% of its initial value. This result indicates that the structure stability of the nanoporous surface alloy is significantly higher than that of

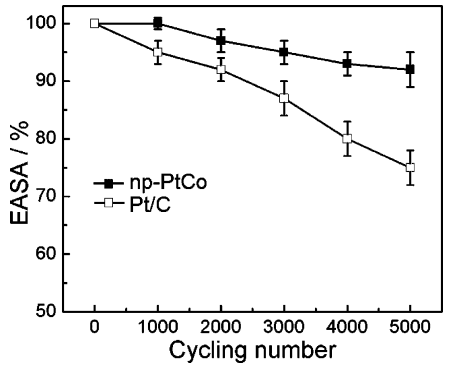

Figure 5. Effect of continuous CV cycling from 0.6 to 0.9 V in a 0.5 M H_2SO_4 solution on the EASA of the np-PtCo surface alloy and Pt/C.

Pt/C despite the incorporation of a more active metal Co. The SEM images of the np-PtCo surface alloy before and after 5000 CV cycles are shown in Figure 6. It is observed that after

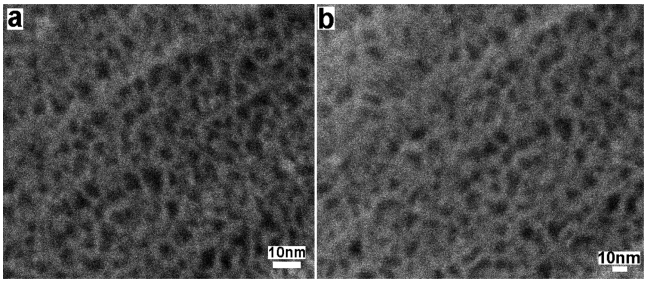

Figure 6. SEM images of the np-PtCo surface alloy before (a) and after (b) 5000 CV cycles from 0.6 to 0.9 V.

cycling the bicontinuous ligament−pore structure is well retained and the ligaments are only slightly coarsened (most of ligament sizes are still less than 10 nm; Figure 6b). The surface diffusion scaling follows a power law decay (proportional to a quarter order of time); thus, the structure coarsening of porous metals is significantly retarded as the ligament size grows larger, especially for Pt that has a rather small surface diffusivity.[51] Moreover, it has been demonstrated that a reduced Pt−Pt interatomic distance (i.e., Pt lattice contraction) can enhance the durability of the Pt catalyst.[62] On the basis of these arguments, it is no surprise that the uniquely strained Pt-rich surface alloy structure exhibits excellent stability against coarsening.

CONCLUSIONS

This study demonstrates that a 3D bicontinuous np-PtCo alloy with uniform alloy composition and ligament size can be facilely prepared by dealloying a PtCoAl ternary alloy. Moreover, by mild electrochemical dealloying, np-PtCo can be converted to a np-PtCo near-surface alloy that shows superior electrocatalytic activity and durability toward MOR. It is suggested that the surface strain and alloying effect would result in more active surface sites that are responsible for the enhanced performance. With the advantages of enhanced catalytic activity, high durability, and simple fabrication, this strategy can also be used to prepare other low-cost nanoporous alloy systems, and the obtained nanomaterials with high structure stability and large surface area are very promising for applications in energy- and catalysis-related areas.

■ ASSOCIATED CONTENT

Supporting Information

Additional figures (EDS spectra and CV and electrochemical CO-stripping curves). This material is available free of charge via the Internet at http://pubs.acs.org.

■ AUTHOR INFORMATION

Corresponding Author

*E-mail: qiuhuajun@gmail.com.

Notes

The authors declare no competing financial interest.

■ ACKNOWLEDGMENTS

This work was supported by Nanyang Technological University and Shandong University. H.Q. thanks the two reviewers for their insightful advice.

■ REFERENCES

(1) Adzic, R. R.; Kowal, A.; Li, M.; Shao, M.; Sasaki, K.; Vukmirovic, M. B.; Zhang, J.; Marinkovic, N. S.; Liu, P.; Frenkel, A. I. *Nat. Mater.* **2009**, *8*, 325−330.

(2) Liu, L. F.; Pippel, E.; Scholz, R.; Gosele, U. *Nano Lett.* **2009**, *9*, 4352−4358.

(3) Gasteiger, H. A.; Kocha, S. S.; Sompalli, B.; Wagner, F. T. *Appl. Catal., B* **2005**, *56*, 9−35.

(4) Hsieh, C. T.; Lin, J. Y. *J. Power Sources* **2009**, *188*, 347−352.

(5) Stamenkovic, V. R.; Mun, B. S.; Arenz, M.; Mayrhofer, K. J. J.; Lucas, C. A.; Wang, G. F.; Ross, P. N.; Markovic, N. M. *Nat. Mater.* **2007**, *6*, 241−247.

(6) Hernandez-Fernandez, P.; Montiel, M.; Ocon, P.; Fierro, J. L. G.; Wang, H.; Abruna, H. D.; Rojas, S. *J. Power Sources* **2010**, *195*, 7959−7967.

(7) Li, W. Z.; Wang, X.; Chen, Z. W.; Waje, M.; Yan, Y. S. *J. Phys. Chem. B* **2006**, *110*, 15353−15358.

(8) Kuo, P. L.; Hsu, C. H. *ACS Appl. Mater. Interfaces* **2011**, *3*, 115−118.

(9) Chen, A.; Holt-Hindle, P. *Chem. Rev.* **2010**, *110*, 3767−3804.

(10) Borup, R.; Meyers, J.; Pivovar, B.; Kim, Y. S.; Mukundan, R.; Garland, N.; Myers, D.; Wilson, M.; Garzon, F.; Wood, D.; Zelenay, P.; More, K.; Stroh, K.; Zawodzinski, T.; Boncella, J.; McGrath, J. E.; Inaba, M.; Miyatake, K.; Hori, M.; Ota, K.; Ogumi, Z.; Miyata, S.; Nishikata, A.; Siroma, Z.; Uchimoto, Y.; Yasuda, K.; Kimijima, K.; Iwashita, N. *Chem. Rev.* **2007**, *107*, 3904−3951.

(11) Wang, Z. B.; Yin, G. P.; Zhang, J.; Sun, Y. C.; Shi, P. F. *Electrochim. Acta* **2006**, *51*, 5691−5697.

(12) Su, F.; Zeng, J.; Bao, X.; Yu, Y.; Lee, J. Y.; Zhao, X. S. *Chem. Mater.* **2005**, *17*, 3960−3967.

(13) Okaya, K.; Yano, H.; Uchida, H.; Watanabe, M. *ACS Appl. Mater. Interfaces* **2010**, *2*, 888−895.

(14) Chen, Z. W.; Waje, M.; Li, W. Z.; Yan, Y. S. *Angew. Chem., Int. Ed.* **2007**, *46*, 4060−4063.

(15) Sun, S. H.; Zhang, G. X.; Geng, D. S.; Chen, Y. G.; Li, R. Y.; Cai, M.; Sun, X. L. *Angew. Chem., Int. Ed.* **2011**, *50*, 422−426.

(16) Liang, H. W.; Cao, X. A.; Zhou, F.; Cui, C. H.; Zhang, W. J.; Yu, S. H. *Adv. Mater.* **2011**, *23*, 1467−1471.

(17) Wang, C.; van der Vliet, D.; Chang, K.-C.; You, H.; Strmcnik, D.; Schlueter, J. A.; Markovic, N. M.; Stamenkovic, V. R. *J. Phys. Chem. C* **2009**, *113*, 19365−19368.

(18) Koenigsmann, C.; Zhou, W.-p.; Adzic, R. R.; Sutter, E.; Wong, S. S. *Nano Lett.* **2010**, *10*, 2806−2811.

(19) Guo, S.; Zhang, S.; Sun, X.; Sun, S. *J. Am. Chem. Soc.* **2011**, *133*, 15354−15357.

(20) Shui, J. I.; Chen, C.; Li, J. C. M. *Adv. Funct. Mater.* **2011**, *21*, 3357−3362.

(21) Koenigsmann, C.; Santulli, A. C.; Gong, K. P.; Vukmirovic, M. B.; Zhou, W. P.; Sutter, E.; Wong, S. S.; Adzic, R. R. *J. Am. Chem. Soc.* **2011**, *133*, 9783−9795.

(22) Koenigsmann, C.; Santulli, A. C.; Sutter, E.; Wong, S. S. *ACS Nano* **2011**, *5*, 7471−7487.

(23) Strasser, P.; Koh, S.; Anniyev, T.; Greeley, J.; More, K.; Yu, C. F.; Liu, Z. C.; Kaya, S.; Nordlund, D.; Ogasawara, H.; Toney, M. F.; Nilsson, A. *Nat. Chem.* **2010**, *2*, 454−460.

(24) Stamenkovic, V. R.; Mun, B. S.; Mayrhofer, K. J. J.; Ross, P. N.; Markovic, N. M. *J. Am. Chem. Soc.* **2006**, *128*, 8813−8819.

(25) Liu, Z.; Su, F.; Zhang, X.; Tay, S. W. *ACS Appl. Mater. Interfaces* **2011**, *3*, 3824−3830.

(26) Liu, J.; Cao, L.; Huang, W.; Li, Z. *ACS Appl. Mater. Interfaces* **2011**, *3*, 3552−3558.

(27) Stamenkovic, V.; Mun, B. S.; Mayrhofer, K. J. J.; Ross, P. N.; Markovic, N. M.; Rossmeisl, J.; Greeley, J.; Norskov, J. K. *Angew. Chem., Int. Ed.* **2006**, *45*, 2897−2901.

(28) Koh, S.; Leisch, J.; Toney, M. F.; Strasser, P. *J. Phys. Chem. C* **2007**, *111*, 3744−3752.

(29) Komatsu, T.; Tamura, A. *J. Catal.* **2008**, *258*, 306−314.

(30) Zeng, J.; Lee, J. Y. *Int. J. Hydrogen Energy* **2007**, *32*, 4389−4396.

(31) Gojkovic, S. L. *J. Serb. Chem. Soc.* **2003**, *68*, 859−870.

(32) Salgado, J. R. C.; Antolini, E.; Gonzalez, E. R. *Appl. Catal., B* **2005**, *57*, 283−290.

(33) Erlebacher, J.; Aziz, M. J.; Karma, A.; Dimitrov, N.; Sieradzki, K. *Nature* **2001**, *410*, 450−453.

(34) Ding, Y.; Kim, Y. J.; Erlebacher, J. *Adv. Mater.* **2004**, *16*, 1897−1900.

(35) Qiu, H. J.; Xu, C. X.; Huang, X. R.; Ding, Y.; Qu, Y. B.; Gao, P. J. *J. Phys. Chem. C* **2008**, *112*, 14781−14785.

(36) Chen, L. Y.; Yu, J. S.; Fujita, T.; Chen, M. W. *Adv. Funct. Mater.* **2009**, *19*, 1221−1226.

(37) Qian, L. H.; Chen, M. W. *Appl. Phys. Lett.* **2007**, *91*, 083105.

(38) Qiu, H.; Zhang, Z.; Huang, X.; Qu, Y. *ChemPhysChem* **2011**, *12*, 2118−2123.

(39) Qiu, H. J.; Xu, C. X.; Huang, X. R.; Ding, Y.; Qu, Y. B.; Gao, P. J. *J. Phys. Chem. C* **2009**, *113*, 2521−2525.

(40) Fujita, T.; Okada, H.; Koyama, K.; Watanabe, K.; Maekawa, S.; Chen, M. W. *Phys. Rev. Lett.* **2008**, *101*, 166601.

(41) Zhang, Z. H.; Wang, Y.; Qi, Z.; Zhang, W. H.; Qin, J. Y.; Frenzel, J. *J. Phys. Chem. C* **2009**, *113*, 12629−12636.

(42) Zhang, Z. H.; Wang, Y.; Wang, X. G. *Nanoscale* **2011**, *3*, 1663−1674.

(43) Zielasek, V.; Jurgens, B.; Schulz, C.; Biener, J.; Biener, M. M.; Hamza, A. V.; Baumer, M. *Angew. Chem., Int. Ed.* **2006**, *45*, 8241−8244.

(44) Wang, D.; Zhao, P.; Li, Y. *Sci. Rep.* **2012**, DOI: 10. 1038/srep00037.

(45) Liu, L. F.; Scholz, R.; Pippel, E.; Gosele, U. *J. Mater. Chem.* **2010**, *20*, 5621−5627.

(46) Du, C.; Chen, M.; Wang, W.; Yin, G. *ACS Appl. Mater. Interfaces* **2010**, *3*, 105−109.

(47) Liu, Z. N.; Huang, L. H.; Zhang, L. L.; Ma, H. Y.; Ding, Y. *Electrochim. Acta* **2009**, *54*, 7286−7293.

(48) Stephens, I. E. L.; Bondarenko, A. S.; Perez-Alonso, F. J.; Calle-Vallejo, F.; Bech, L.; Johansson, T. P.; Jepsen, A. K.; Frydendal, R.; Knudsen, B. P.; Rossmeisl, J.; Chorkendorff, I. *J. Am. Chem. Soc.* **2011**, *133*, 5485−5491.

(49) Xu, C.; Liu, Y.; Wang, J.; Geng, H.; Qiu, H. *ACS Appl. Mater. Interfaces* **2011**, *3*, 4626−4632.

(50) Van Petegem, S.; Brandstetter, S.; Maass, R.; Hodge, A. M.; El-Dasher, B. S.; Biener, J.; Schmitt, B.; Borca, C.; Van Swygenhoven, H. *Nano Lett.* **2009**, *9*, 1158−1163.

(51) Erlebacher, J. *J. Electrochem. Soc.* **2004**, *151*, C614−C626.

(52) Sieradzki, K. *J. Electrochem. Soc.* **1993**, *140*, 2868−2872.

(53) Simmonds, M. C.; Kheyrandish, H.; Colligon, J. S.; Hitchman, M. L.; Cade, N.; Iredale, J. *Corros. Sci.* **1998**, *40*, 43−48.

(54) Knudsen, J.; Nilekar, A. U.; Vang, R. T.; Schnadt, J.; Kunkes, E. L.; Dumesic, J. A.; Mavrikakis, M.; Besenbacher, F. *J. Am. Chem. Soc.* **2007**, *129*, 6485−6490.
(55) Koh, S.; Strasser, P. *J. Am. Chem. Soc.* **2007**, *129*, 12624−12625.
(56) Mani, P.; Srivastava, R.; Strasser, P. *J. Power Sources* **2011**, *196*, 666−673.
(57) Zhou, W. P.; Li, M.; Koenigsmann, C.; Ma, C.; Wong, S. S.; Adzic, R. R. *Electrochim. Acta* **2011**, *56*, 9824−9830.
(58) Wieckowski, A.; Rubel, M.; Gutierrez, C. *J. Electroanal. Chem.* **1995**, *382*, 97−101.
(59) Prabhuram, J.; Zhao, T. S.; Tang, Z. K.; Chen, R.; Liang, Z. X. *J. Phys. Chem. B* **2006**, *110*, 5245−5252.
(60) Kabbabi, A.; Faure, R.; Durand, R.; Beden, B.; Hahn, F.; Leger, J. M.; Lamy, C. *J. Electroanal. Chem.* **1998**, *444*, 41−53.
(61) Guo, J. W.; Zhao, T. S.; Prabhuram, J.; Chen, R.; Wong, C. W. *Electrochim. Acta* **2005**, *51*, 754−763.
(62) Wang, J. X.; Ma, C.; Choi, Y.; Su, D.; Zhu, Y.; Liu, P.; Si, R.; Vukmirovic, M. B.; Zhang, Y.; Adzic, R. R. *J. Am. Chem. Soc.* **2011**, *133*, 13551−13557.